A Dynamic Marine Calcium Cycle During the Past 28 Million Years

Elizabeth M. Griffith, *et al.*

Science **322**, 1671 (2008);
DOI: 10.1126/science.1163614

Science (print ISSN 0036-8075; online ISSN 1095-9203) is published weekly, except the last week in December, by the American Association for the Advancement of Science, 1200 New York Avenue NW, Washington, DC 20005.

This intramolecular looping mechanism resembles that of a ring-closure reaction (MP→C_{a*} in Fig. 3E), and the threading rate will therefore depend on the effective molarity (EM) of the reactive components (the cavity and the open chain end). The EM (*23*) describes the relative ease of ring-closure reactions compared with intermolecular reactions under otherwise identical conditions and has been tabulated in the literature (*24*). EM values contain all the intrinsic parameters of chains relevant for ring closure such as ring strain and torsional entropy. In line with intuition, EM values become smaller when the chains connecting the reactive components become longer. According to the model (Fig. 3E), the intramolecular path will be more favored than the intermolecular path as long as $K_aEM > 1$, in which K_a is the association constant of the outside-viologen complex. At the given values of K_a (≈40 M^{-1}), these conditions are met for chains shorter than 40 atoms (because $EM = 0.025$ M for chains of 40 atoms), which is in line with the observation that the polymer chains (90 to 440 atoms) apparently do not benefit from this looping process. The intramolecular process will not only be lower in transition state energy than the intermolecular process but also energetically downhill in the direction of the viologen trap. In the process of moving along the chain toward the viologen moiety ($C_{a*} \rightarrow C_{b*} \rightarrow C_{c*}$ in Fig. 3E), the chain length between the reactive components (the outside of the macrocycle and the viologen moiety) decreases, and the EM value consequently increases ($EM_a < EM_b < EM_c$), resulting in a downhill reaction coordinate (Fig. 3C). The resulting unidirectional movement continues until the loop becomes too small (C_{c*}, Fig. 3, C and E) and the viologen dissociates from the outside of the macrocycle, after which the last eight atoms are traversed in a nonstabilized fashion and the macrocycle embraces the viologen trap. As a result, the traversing of the last eight atoms becomes rate-limiting, which is in agreement with the experimental results that the observed rates never become significantly higher than the rate of traversing a chain of eight atoms (Fig. 2).

To further support the model, we synthesized two different porphyrin macrocycles (**2**-H_2 and **2**-Zn) (*25*) with -OH functionalities on the outside of the cavity, which form stronger outside complexes with **Vdb** [$K_a = 2 \times 10^4$ M^{-1} and 5×10^4 M^{-1} for **2**-Zn and **2**-H_2, respectively; see figs. S9, S10, and accompanying text (*16*)]. This modification was expected to result in higher threading rates over the polymer chains as well because $K_aEM > 1$ in a larger region of chain lengths. It should be noted that, even at these high association constants, quenching caused by the outside complexes is less than 5% of the total measured quenching at the applied experimental concentrations (fig. S11). The fluorescence threading studies of **2**-H_2 and **2**-Zn revealed that both **2**-H_2 and **2**-Zn traverse the short chains and the oligomer chains in an analogous fashion to **1**-H_2 and **1**-Zn (Fig. 2 inset and Table 1). However, the threading over the polymer chains is significantly faster for both **2**-H_2 (on average 2.2 times) and **2**-Zn (up to a factor of 4). These results thus support the idea that the higher affinity of **2**-H_2 and **2**-Zn for the viologen moiety on the outside of the macrocycle enhances the rates of threading over the polymer chains via the intramolecular looping process.

The experimentally determined length dependencies for the threading process can be described by a modified consecutive hopping model, which includes a kinetically favorable so-called entron effect. The above results highlight that weak supramolecular interactions between the outside of the macrocycle and the chain have a dramatic effect on the overall threading process. It is a classical example of how small interactions can lead to accelerated rates by means of transition state stabilization. In our simple biomimetic model system, these interactions both initiate and guide the threading process, resulting in accelerated rates and mimicking the natural translocation systems in which interactions between the biopolymer and a receptor in the vicinity of the pore are fundamental and essential steps in efficient and selective translocation (*12*, *13*). Given that our studies show that even weak interactions between the macrocyclic exterior and the polymer chains already cause significant increases in the threading rates, it is very likely that such assisted threading mechanisms not only play a role in the specific natural examples but also in a much larger number of natural polymer translocation systems. Another intriguing effect of the mechanism is that unidirectional motion (achieved without the application of an external driving force) is facilitated toward the trapping site. This driving force should allow for the design of novel artificial machines (*26*) and catalysts in which the threading can be finely controlled.

References and Notes

1. W. Wickner, R. Schekman, *Science* **310**, 1452 (2005).
2. E. J. Mancini *et al.*, *Cell* **118**, 743 (2004).
3. A. Johnson, M. O'Donnell, *Annu. Rev. Biochem.* **74**, 283 (2005).
4. E. R. Kay, D. A. Leigh, F. Zerbetto, *Angew. Chem. Int. Ed.* **46**, 72 (2007).
5. R. A. Bissell, E. Cordova, A. E. Kaifer, J. F. Stoddart, *Nature* **369**, 133 (1994).
6. A. M. Brouwer *et al.*, *Science* **291**, 2124 (2001); published online 22 February 2001 (10.1126/science.1057886).
7. J. D. Badjic, V. Balzani, A. Credi, S. Silvi, J. F. Stoddart, *Science* **303**, 1845 (2004).
8. E. R. Kay, D. A. Leigh, *Nature* **440**, 286 (2006).
9. M. C. Jiménez, C. Dietrich-Buchecker, J.-P. Sauvage, *Angew. Chem. Int. Ed.* **39**, 3284 (2000).
10. Y. Liu *et al.*, *J. Am. Chem. Soc.* **127**, 9745 (2005).
11. P. Thordarson, E. J. A. Bijsterveld, A. E. Rowan, R. J. M. Nolte, *Nature* **424**, 915 (2003).
12. G. Blobel, *ChemBioChem* **1**, 86 (2000).
13. T. A. Rapoport, *Nature* **450**, 663 (2007).
14. R. G. E. Coumans, J. A. A. W. Elemans, R. J. M. Nolte, A. E. Rowan, *Proc. Natl. Acad. Sci. U.S.A.* **103**, 19647 (2006).
15. P. Hidalgo Ramos *et al.*, *J. Am. Chem. Soc.* **129**, 5699 (2007).
16. Materials and methods are detailed in supporting online material available at *Science* Online.
17. W. Herrmann, B. Keller, G. Wenz, *Macromolecules* **30**, 4966 (1997).
18. A. Harada, J. Li, M. Kamachi, *Nature* **356**, 325 (1992).
19. L. P. Hammett, *Physical Organic Chemistry* (McGraw-Hill, New York, ed. 2, 1970), p. 112.
20. A. B. Kolomeisky, *Biophys. J.* **94**, 1547 (2008).
21. E. Slonkina, A. B. Kolomeisky, *J. Chem. Phys.* **118**, 7112 (2003).
22. A. Meller, L. Nivon, D. Branton, *Phys. Rev. Lett.* **86**, 3435 (2001).
23. L. Mandolini, *Adv. Phys. Org. Chem.* **22**, 1 (1986).
24. C. Galli, L. Mandolini, *Eur. J. Org. Chem.* 3117 (2000).
25. P. Thordarson *et al.*, *J. Am. Chem. Soc.* **125**, 1186 (2003).
26. W. R. Browne, B. L. Feringa, *Nat. Nanotechnol.* **1**, 25 (2006).

27. This research was supported by a National Research School Combination Catalysis Controlled by Chemical Design grant, Nederlandse Organisatie voor Wetenschappelijk Onderzoek Veni, Vidi and Vici grants (J.A.A.W.E. and A.E.R.), a Koninklijke Nederlandse Akademie van Wetenschappen grant (R.J.M.N.), and a Nanoned grant (A.E.R. and R.J.M.N.).

Supporting Online Material

www.sciencemag.org/cgi/content/full/322/5908/1668/DC1
Materials and Methods
Figs. S1 to S18
Table S1
References

14 August 2008; accepted 14 November 2008
10.1126/science.1164647

A Dynamic Marine Calcium Cycle During the Past 28 Million Years

Elizabeth M. Griffith,[1,2]* Adina Paytan,[2] Ken Caldeira,[3] Thomas D. Bullen,[4] Ellen Thomas[5,6]

Multiple lines of evidence have shown that the isotopic composition and concentration of calcium in seawater have changed over the past 28 million years. A high-resolution, continuous seawater calcium isotope ratio curve from marine (pelagic) barite reveals distinct features in the evolution of the seawater calcium isotopic ratio suggesting changes in seawater calcium concentrations. The most pronounced increase in the $\delta^{44/40}$Ca value of seawater (of 0.3 per mil) occurred over roughly 4 million years following a period of low values around 13 million years ago. The major change in marine calcium corresponds to a climatic transition and global change in the carbon cycle and suggests a reorganization of the global biogeochemical system.

The marine calcium (Ca^{2+}) cycle is related to processes that control oceanic alkalinity and atmospheric CO_2, playing an important role in earth's climate (*1*). Calcium carbonate ($CaCO_3$) sedimentation in the ocean represents the largest carbon sink in the combined atmosphere, biosphere, and ocean system, and thus strongly influences the global carbon cycle (*2*). Fluctuations in $CaCO_3$ sedimentation reflect imbalances in the long-term

carbon cycle and are related to global changes in climate and tectonics (*3*). Such fluctuations may also be reflected in the marine Ca^{2+} cycle and seawater Ca^{2+} concentrations and isotopic ratios (*4*, *5*).

Changes in Ca^{2+} concentration of seawater throughout the Phanerozoic are revealed in brine inclusions (*6*, *7*), elemental ratios in marine skeletal carbonates (*8*), and the changing abundance of carbonate and potash-evaporite minerals (*9*, *10*). Shifts in seawater Ca^{2+} concentration during the past 28 million years (My) are thought to reflect predominantly sedimentological factors (e.g., carbonate deposition and dolomitization) (*11*), although changes in sea-floor generation rates may also play a role (*12*).

The amount of Ca^{2+} in the modern ocean and its isotopic composition [$\delta^{44/40}Ca_{seawater}$ (*13*)] are determined by the balance between riverine and hydrothermal inputs and removal through $CaCO_3$ deposition and alteration of oceanic crust and their respective isotopic compositions (fig. S1). Estimates for the isotopic composition of Ca^{2+} inputs from continental rivers range from $\delta^{44/40}Ca$ = –0.87 to –1.30 per mil (‰) (*5*, *14*–*16*); hydrothermal inputs average –0.96 ± 0.20‰ (*15*). When $CaCO_3$ is precipitated from seawater, its Ca-isotopic composition is 0.7 to 1.6‰ less than that of dissolved Ca^{2+} in seawater, depending on which mineral, calcite or aragonite, is precipitated and on parameters such as temperature and precipitation rate (*17*). Alteration of oceanic crust, estimated to account for less than 10% of the Ca^{2+} sink in the modern ocean, has an average $\delta^{44/40}Ca$ between 0.7 and 1.7‰ less than $\delta^{44/40}Ca_{seawater}$ (*18*). Due to the range of isotopic signatures in the modern ocean and the uncertainty of the representative average values, it is not known precisely whether or over what time scale the marine Ca^{2+} cycle is in isotopic steady state (*5*, *14*, *15*, *19*).

Recent work using Ca-isotopic ratios measured in marine carbonates (*14*, *16*, *19*–*21*) has shown that the isotopic signature recorded in carbonates fluctuated over time. However, there is no consensus as to whether seawater composition or environmental and physiological factors ultimately control the Ca-isotopic composition measured in marine carbonates (*16*, *19*). We present a high-resolution, continuous seawater Ca-isotope curve from marine (pelagic) barite ($BaSO_4$) to help explain factors controlling the cycles of calcium and carbon over the past 28 My.

Marine barite, a minor component of marine sediments, is a useful recorder of changes in seawater chemistry (*22*–*24*). Calcium (Ca^{2+}) substitutes for barium (Ba^{2+}) in the barite crystal lattice, providing an archive of Ca-isotopes in a highly stable sulfate mineral (*25*). Marine barite has advantages over carbonate minerals for studying the seawater Ca-isotopic ratio because of its resistance to diagenesis in oxic pelagic sediments and its uninterrupted record over important climate intervals associated with carbonate dissolution (*22*). In addition, marine barite precipitates inorganically in seawater; thus, no physiological "vital effects" are expected (*22*).

The measured $\delta^{44/40}Ca$ of Holocene marine barite separated from more than 20 core-top deep sea sediment samples in the major ocean basins are indistinguishable from each other, with a $\delta^{44/40}Ca$ of –2.01 ± 0.15‰ (average $2\sigma_{mean}$) (*25*). The offset from seawater (isotopic fractionation) is not strongly related to any measured environmental parameter (*25*) and encompasses the expected range of conditions over the past 28 My at the location of our down-core samples. This offset can therefore be considered constant during the past 28 My (*26*).

The seawater Ca-isotope curve for the past 28 My was reconstructed from marine barite at a resolution better than 1 My from 51 sediment samples collected by the Deep Sea Drilling Project (DSDP) and the Ocean Drilling Program (ODP) at sites 572 to 575, 1218, and 1219 in the east equatorial Pacific (*27*).

The marine barite $\delta^{44/40}Ca_{seawater}$ record (Fig. 1) displays a long-term trend toward more positive values, in general agreement with existing seawater Ca-isotope records from biogenic carbonates (Fig. 1 and table S1). However, our data also reveal features that correspond with shifts in the marine carbon and oxygen isotope records (Fig. 1). The $\delta^{44/40}Ca_{seawater}$ remained fairly stable at around –0.3‰ ± 0.1‰ ($2\sigma_{mean}$, n = 26) from 28 million years ago (Ma) until around 13 Ma. From 13 Ma to 8 Ma, it rose to the modern value, where it remained until the present (0 ± 0.1‰, $2\sigma_{mean}$, n = 23).

We use a numerical model to investigate the implications of this Ca-isotope record for the marine calcium biogeochemical cycle in relation to major climatic events and perturbations in the carbon cycle [following (*14*); for details, see (*27*)]. The state variables in the model are the isotopic composition of seawater Ca^{2+} (model input from the barite data) and its concentration. Model parameters include the isotopic signature of the combined input flux of Ca^{2+} (riverine, hydrothermal, and dolomitization) and the isotopic fractionation during $CaCO_3$ precipitation. The oceanic residence time of Ca^{2+} is taken to be 1.3 My (*21*) and assumed to be constant (*28*). Using a constant sedimentation flux (and changing residence time) did not drastically vary the pattern in calculated Ca^{2+} concentrations (*27*).

An initial condition for 28 Ma is constructed in the model, and the set of equations are solved simultaneously, so the system is allowed to evolve

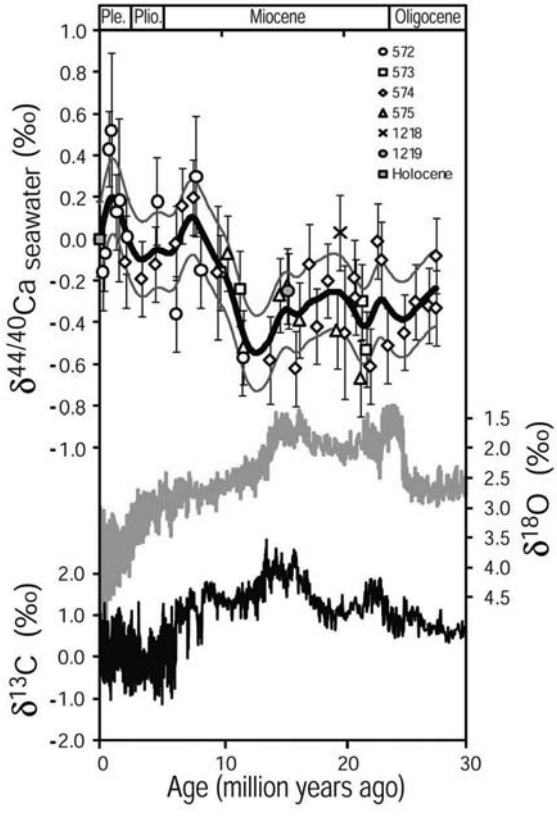

Fig. 1. Ca-isotopic composition of seawater ($\delta^{44/40}Ca_{seawater}$) over the past 28 My. All the Ca-isotopic ratios are reported in per mil relative to seawater and are plotted with respect to the chronology in (*33*) [see (*27*)]. Error bars are the precision of each sample calculated as the $2\sigma_{mean}$ of replicate analyses on the thermal ionization mass spectrometer or the average $2\sigma_{mean}$ if only one analysis was made. The bold solid black curve is the cubic smoothing spline of the data (*34*) with ± 0.18‰ (average $2\sigma_{mean}$) in gray. Two samples with $2\sigma_{mean}$ > 0.4‰ were removed from the trend and figure. Averages of duplicate samples are plotted. Smoothed global $\delta^{18}O$ and $\delta^{13}C$ synthesis of benthic (deep sea) foraminifera reported relative to Pee Dee belemnite in per mil (*35*). Pleistocene, Ple.; Pliocene, Plio.

[1]Department of Geological and Environmental Sciences, Stanford University, Building 320, Room 118, Stanford, CA 94305, USA. [2]Institute of Marine Sciences, University of California, Santa Cruz, CA 95064, USA. [3]Department of Global Ecology, Carnegie Institution of Washington, 260 Panama Street, Stanford, CA 94305, USA. [4]Branch of Regional Research, Water Resources Division, U.S. Geological Survey, MS 420, 345 Middlefield Road, Menlo Park, CA 94025, USA. [5]Department of Geology and Geophysics, Yale University, Post Office Box 208109, New Haven, CT 06520, USA. [6]Department of Earth and Environmental Sciences, Wesleyan University, 265 Church Street, Middletown, CT 06459, USA.

*To whom correspondence should be addressed. E-mail: egriffith@ucsc.edu

toward the present. In the model, the assumption of constant average values estimated for the present-day Ca^{2+} system (sources and sinks) (fig. S1) leads to unacceptable seawater Ca^{2+} fluctuations. Accordingly, the isotopic composition of the input flux of Ca^{2+} ($\delta^{44/40}Ca_{in}$) and/or the isotopic fractionation associated with the sink ($\Delta^{44/40}Ca_{sed}$) must have varied over this time period. First, we varied $\delta^{44/40}Ca_{in}$ with time (Fig. 2A), constrained at points where the Ca^{2+} concentration is known from measurements of brine inclusions (*7*) and linearly extrapolated between these points as described in (*27*).

Because the first approach assumes time-dependent isotopic variation in the input flux (Fig. 2A), the general long-term trend in the Ca-isotopic composition of seawater is directly related to changes in the isotopic signature of this flux. With these assumptions, a shift in $\delta^{44/40}Ca_{in}$ to more positive values likely reflects a shift in the weathered terrain to more continental sourced silicate rocks with a more positive $\delta^{44/40}Ca$ value (*16*). An increase from 6% to 17% in the contribution of silicate weathering to the total weathering flux can explain the data (*27*). The $\delta^{44/40}Ca$ value of carbonates subjected to weathering also changes, contributing about 0.1‰ of the 0.6‰ long-term increase in the modeled $\delta^{44/40}Ca_{in}$ over this time period (*20*).

Dolomitization (a source of Ca^{2+} to the oceans) could have influenced $\delta^{44/40}Ca_{in}$ in the past. Dolomitization releases Ca^{2+} by diffusional exchange with Mg^{2+}, adding Ca^{2+} depleted in ^{44}Ca without affecting the seawater carbonate flux (*19*). The rate of marine dolomite formation has decreased over the Cenozoic to a present minimum (*11*), consistent with the increasing $\delta^{44/40}Ca_{seawater}$ over the past 28 My, but it is unclear how important this process has been as a source of Ca^{2+} during this time interval or over the observed transition about 13 Ma.

In addition, the isotopic fractionation associated with the sink ($\Delta^{44/40}Ca_{sed}$) likely changed. Shifts in the $\Delta^{44/40}Ca_{sed}$ could have been caused by changes in temperature during precipitation, rate of precipitation, or in the mineralogy of the deposited carbonates (aragonite versus calcite), which is controlled by the dominant calcifying organisms (*10*, *20*). In the second approach (Fig. 2B), $\Delta^{44/40}Ca_{sed}$ varies and is calculated as the difference between seawater values in this study and the bulk carbonate (output) record of (*21*). $\delta^{44/40}Ca_{in}$ also varies, as in the first model, and is likewise constrained by the long-term trend in seawater Ca^{2+} concentration from fluid inclusions (*27*). This results in a slightly different $\delta^{44/40}Ca_{in}$ reconstruction due to the differences in $\Delta^{44/40}Ca_{sed}$ histories we used. Changing the $\Delta^{44/40}Ca_{sed}$ in addition to $\delta^{44/40}Ca_{in}$ does not in general change the shape of the modeled seawater Ca^{2+} concentration curve.

In summary, model results indicate that the isotopic composition of the combined input flux of Ca^{2+} and/or isotopic fractionation during carbonate precipitation must have changed over the past 28 My (*21*, *16*), and these results suggest changes in seawater Ca^{2+} concentrations. Specifically, the relatively abrupt (<5 My) changes in the $\delta^{44/40}Ca_{seawater}$ curve indicate large, rapid transient changes in the amount of Ca^{2+} in the ocean, of up to twice the present value (Fig. 2), and/or transient fluctuations in the Ca-isotopic composition of the input or sedimentation fluxes of up to 1‰. However, such large and abrupt changes in the Ca-isotopic compositions of these input or output fluxes is outside the range of measured present-day values (*5*, *14*–*16*) and does not seem to be a likely mechanism for explaining all variation in our seawater Ca-isotope record.

The most prominent change in the oceanic Ca^{2+} concentration corresponds to a major climatic transition at ~13 Ma (middle Miocene), when the earth's climate changed from a period of relative global warmth into a cooler climate, while the Antarctic ice sheet increased in volume (*29*). This increase in Ca^{2+} concentration may be a consequence of an increase in the Ca^{2+} flux to the ocean.

An increase in the Ca^{2+} flux from continental weathering (without an accompanying increase in carbonate deposition) from recently exposed continental shelves, increased weathering, and/or transport of weathered material into the oceans associated with glaciation might have resulted from a drop in sea level as shown by the sharp 0.5‰ increase in the $\delta^{18}O$ of benthic foraminifera (*30*) (Fig. 1). Increased weathering of carbonate sediments (relative to silicate sediments) increases the flux of Ca^{2+} to the ocean relative to the carbon (C) flux providing a potential means for decoupling the Ca^{2+} and C systems (*19*). The rate of change in the Ca^{2+} flux must be decoupled from and higher than the rate of change in the flux of C; otherwise, Ca^{2+} flux variations are quickly (<<1 My) buffered by feedbacks involving terrestrial rock weathering and marine C-$CaCO_3$ deposition/dissolution processes.

The calcium carbonate compensation depth (CCD), the water depth where the calcite rain rate is balanced by its dissolution rate such that all calcite produced in the water column is dissolved, records the balance between $CaCO_3$ deposition/dissolution in deep sea sediments (*31*). Shifts in the CCD occurred during the past 28 My (*31*), resulting from changes in deep ocean chemistry and the supply rate of $CaCO_3$ to the sediments, but long-term changes in the equatorial Pacific CCD (>1 My) do not appear to be solely controlled by oceanic Ca^{2+} concentrations (fig. S7).

A change in the marine carbon cycle occurred during the middle Miocene climatic transition, when the carbon isotopic composition of bulk carbonates ($\delta^{13}C_{carb}$) began to decrease by about 2‰ to modern values (*30*) (Fig. 1). If the total C flux to the ocean had been constant, this would have implied a shift to more continental-sourced

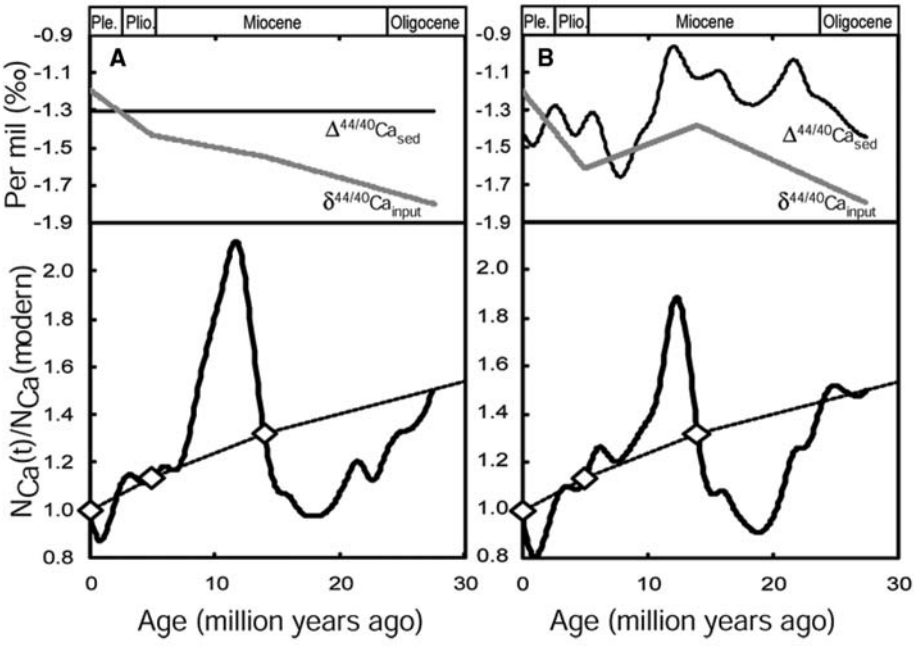

Fig. 2. Time varying isotopic composition of the calcium input flux to the oceans ($\delta^{44/40}Ca_{in}$) and isotopic fractionation during calcium carbonate precipitation before sedimentation ($\Delta^{44/40}Ca_{sed}$) in per mil used in the numerical models (top). Calculated ratio of amount of calcium in the oceans [$N_{Ca}(t)$], relative to the present value [$N_{Ca}(modern)$] constrained using data (open diamonds) from (*7*). Solid black line is $N_{Ca}(t)$ / $N_{Ca}(modern)$; dashed black line is Phanerozoic trend (*7*) (bottom). Numerical model assuming (**A**) constant $\Delta^{44/40}Ca_{sed}$ or (**B**) varying $\Delta^{44/40}Ca_{sed}$ calculated from the difference between seawater $\delta^{44/40}Ca$ (this study) and measured contemporaneous bulk nannofossil ooze carbonates (*14*, *21*).

rocks rich in organic C relative to carbonate weathering over the past ~13 My (*31*). Previous interpretations of $^{87}Sr/^{86}Sr$, $^{187}Os/^{186}Os$, and δ^7Li records agree with a change in the nature of weathered material at this time (*32*).

Many aspects of the biogeochemical Ca^{2+} cycle need to be constrained better by observational and experimental data and paleoceanographic and geologic evidence before a unique interpretation of the causes of the long-term trend and abrupt transitions in $\delta^{44/40}Ca_{seawater}$ is possible. Reconstructions of the global CCD and high-resolution records of seawater Ca^{2+} concentrations (e.g., from fluid inclusions or other proxies) and of the rate of dolomitization and sea-floor generation are all needed.

Our identification of an abrupt middle Miocene change in the $\delta^{44/40}Ca_{seawater}$ record from marine barite attests to the dynamic nature of an element deemed "conservative" in the present ocean and demonstrates that we cannot assume that concentrations of Ca^{2+} in seawater have been stable over the Cenozoic.

References and Notes

1. H. C. Urey, *The Planets, Their Origins and Development* (Yale Univ. Press, New Haven, CT, 1952).
2. A. J. Ridgwell, M. J. Kennedy, K. Caldeira, *Science* **302**, 859 (2003).
3. M. I. Budyko, A. B. Ronov, A. L. Yanshin, *History of the Earth's Atmosphere* (Springer-Verlag, New York, 1987).
4. J. Skulan, D. J. DePaolo, T. L. Owens, *Geochim. Cosmochim. Acta* **61**, 2505 (1997).
5. P. Zhu, J. D. Macdougall, *Geochim. Cosmochim. Acta* **62**, 1691 (1998).
6. T. K. Lowenstein, M. N. Timofeeff, S. T. Brennan, L. A. Hardie, R. V. Demicco, *Science* **294**, 1086 (2001).
7. J. Horita, H. Zimmermann, H. D. Holland, *Geochim. Cosmochim. Acta* **66**, 3733 (2002).
8. J. A. D. Dickson, *Science* **298**, 1222 (2002).
9. P. A. Sandberg, *Nature* **305**, 19 (1983).
10. L. A. Hardie, *Geology* **24**, 279 (1996).
11. H. D. Holland, *Am. J. Sci.* **305**, 220 (2005).
12. C. P. Conrad, C. Lithgow-Bertelloni, *Geology* **35**, 29 (2007).
13. The Ca-isotopic composition of a sample is expressed as the deviation from a standard solution value, using δ-notation in per mil: $\delta^{44/40}Ca = [(^{44}Ca/^{40}Ca_{sample} - ^{44}Ca/^{40}Ca_{standard}) / ^{44}Ca/^{40}Ca_{standard}] \times 1000$, where $^{44}Ca/^{40}Ca_{standard}$ refers to the $^{44}Ca/^{40}Ca$ isotopic ratio of seawater.
14. C. L. De La Rocha, D. J. DePaolo, *Science* **289**, 1176 (2000).
15. A. D. Schmitt, F. Chabaux, P. Stille, *Earth Planet. Sci. Lett.* **213**, 503 (2003).
16. N. G. Sime *et al.*, *Geochim. Cosmochim. Acta* **71**, 3979 (2007).
17. N. Gussone *et al.*, *Geochim. Cosmochim. Acta* **69**, 4485 (2005).
18. M. Amini *et al.*, *Geochim. Cosmochim. Acta* **72**, 4107 (2008).
19. A. Heuser *et al.*, *Paleoceanography* **20**, 10.1029/2004PA001048 (2005).
20. M. S. Fantle, D. J. DePaolo, *Earth Planet. Sci. Lett.* **237**, 102 (2005).
21. J. Farkaš *et al.*, *Geochim. Cosmochim. Acta* **71**, 5117 (2007).
22. A. Paytan, M. Kastner, E. E. Martin, J. D. Macdougall, T. Herbert, *Nature* **366**, 445 (1993).
23. A. Paytan, M. Kastner, D. Campbell, M. H. Thiemens, *Science* **304**, 1663 (2004).
24. A. V. Turchyn, D. P. Schrag, *Science* **303**, 2004 (2004).
25. E. M. Griffith, E. A. Schauble, T. D. Bullen, A. Paytan, *Geochim. Cosmochim. Acta* **72**, 5641 (2008).
26. Range of parameters measured include conditions relevant to the ranges for the measured samples (DSDP-ODP sites): Holocene core-top sample sites include the average annual temperature in the upper 700 m of the water column, where the majority of marine barite is thought to precipitate, 1 to 14°C; the depth of each core-top location, 3175 to 4431 m; water column barite saturation at sea floor, SI = 0.6 to 0.8 and at 700 m, SI = 0.8 to 1.2; average upper (700 m) water column: salinity (34.2 to 34.9), carbonate concentration (86.65 to 139.56 μmol/kg), and dissolved oxygen concentration (1.1 to 6.2 ml/l); bulk sedimentation rate (1.3 to 2.7 cm/thousand years) and barite accumulation rates (0.7 to 23.4 mg m^{-2} $year^{-1}$).
27. Materials and methods are available as supporting material on *Science* Online.
28. A constant residence time in the model requires that the output flux of Ca^{2+} and the total amount of dissolved Ca^{2+} in the oceans vary together. This is a valid assumption if changes in Ca^{2+} concentration occurred due to changes in the input flux of Ca^{2+} to the ocean that are not accompanied with changes in the C cycle. If a change in Ca^{2+} input flux was associated with and compensated by a change in $CaCO_3$ sedimentation through an increase in alkalinity, no change in Ca^{2+} concentration would result. Increasing or decreasing the residence time by 50% gives similar fluctuations but different magnitudes (peak concentrations range from 180% to 290% of present values) (fig. S5). Modeling the Ca^{2+} system with full carbonate chemistry reveals the sensitivity of the Ca^{2+} cycle to changes in C on long time scales (>10,000 years) (*27*). A mechanism for decoupling the two cycles is required in order to result in changes in Ca^{2+} concentration. These might include changes in the rate of dolomitization or the Ca:bicarbonate ratio in the riverine flux due to shifts in the weathering regime.
29. A. Holbourn, W. Kuhnt, M. Schulz, H. Erlenkeuser, *Nature* **438**, 483 (2005).
30. M. Lyle, *Paleoceanography* **18**, 10.1029/2002PA000777 (2003).
31. D. A. Hodell, P. A. Mueller, J. A. McKenzie, G. A. Mead, *Earth Planet. Sci. Lett.* **92**, 165 (1989).
32. E. C. Hathorne, R. H. James, *Earth Planet. Sci. Lett.* **246**, 393 (2006).
33. L. Lourens, F. Hilgen, N. J. Shackleton, J. Laskar, D. Wilson, in *A Geological Time Scale 2004*, F. Gradstein, J. Ogg, A. G. Smith, Eds. (Cambridge Univ. Press, Cambridge, UK, 2004), pp. 409–440.
34. Generated using a smoothing parameter ($P = 0.80$) and data weighted by its precision in the MATLAB 7.6.0.324 (R2008a) cubic smoothing spline function csaps.
35. J. Zachos, M. Pagani, L. Sloan, E. Thomas, K. Billups, *Science* **292**, 686 (2001).

36. Samples provided by the Integrated Ocean Drilling Program. We thank A. Eisenhauer, J. Fitzpatrick, W. A. Griffith, R. Jones, and G. Li for analytical assistance. Supported by NSF CAREER Grant OCE-0449732 (A.P.) and by a National Defense Science and Engineering Graduate Fellowship and an NSF Graduate Research Fellowship (E.M.G.).

Supporting Online Material

www.sciencemag.org/cgi/content/full/322/5908/1671/DC1
Materials and Methods
Figs. S1 to S7
Table S1
References

22 July 2008; accepted 7 November 2008
10.1126/science.1163614

Earthquake Supercycles Inferred from Sea-Level Changes Recorded in the Corals of West Sumatra

Kerry Sieh,[1]* Danny H. Natawidjaja,[2] Aron J. Meltzner,[1] Chuan-Chou Shen,[3] Hai Cheng,[4] Kuei-Shu Li,[3] Bambang W. Suwargadi,[2] John Galetzka,[1] Belle Philibosian,[1] R. Lawrence Edwards[4]

Records of relative sea-level change extracted from corals of the Mentawai islands, Sumatra, imply that this 700-kilometer-long section of the Sunda megathrust has generated broadly similar sequences of great earthquakes about every two centuries for at least the past 700 years. The moment magnitude 8.4 earthquake of September 2007 represents the first in a series of large partial failures of the Mentawai section that will probably be completed within the next several decades.

Large sections of the great arcuate fault beneath the eastern flank of the Indian Ocean have failed progressively over the past 8 years in an extraordinary sequence of big earthquakes (Fig. 1) (*1*–*4*). The largest of these failures of the Sunda megathrust, in 2004, caused the most devastating tsunami the world has seen in many generations. One question of great humanitarian and scientific importance is which remaining unruptured sections of the megathrust will fail next.

Until late 2007, the largest remaining unbroken Sumatran section had been the 700-km-long Mentawai patch, dormant since two great earthquakes in 1797 and 1833 (*5*). Modeling of coral and instrumental geodetic data had shown most of the patch to have been highly coupled throughout at least the past half-century (*6*, *7*). That is, overlying and underlying blocks have been locked together, and strains continue to accumulate. These observations had led to concerns that the remainder of the Mentawai patch might rupture soon (*8*–*11*). In September 2007, rapid-fire failure of portions of the Mentawai patch produced a moment magnitude (M_w) 8.4 earthquake and several large aftershocks (*12*), which served to further elevate anxiety.

[1]Tectonics Observatory, California Institute of Technology, Pasadena, CA 91125, USA. [2]Research Center for Geotechnology, Indonesian Institute of Sciences, Bandung, Indonesia. [3]Department of Geosciences, National Taiwan University, Taipei, Taiwan, ROC. [4]Department of Geology and Geophysics, University of Minnesota, Minneapolis, MN 55455, USA.

*To whom correspondence should be addressed at the Earth Observatory of Singapore, Nanyang Technological University, 639798 Singapore. E-mail: sieh@ntu.edu.sg